Theory of Nernst effect in high-T_c superconductors

Bui Duc Tinh and Baruch Rosenstein
Department of Electrophysics, National Chiao Tung University, Hsinchu 30050, Taiwan, Republic of China
(Received 14 September 2008; published 26 January 2009)

We calculated, using the time-dependent Ginzburg-Landau equation with thermal noise, the transverse thermoelectric conductivity α_{xy} and the Nernst signal e_N, describing the Nernst effect, in type-II superconductor in the vortex-liquid regime. The Gaussian method used is an elaboration of the Hartree-Fock utilized by Ullah and Dorsey [Phys. Rev. Lett. **65**, 2066 (1990)]. An additional assumption often made in analytical calculations that only the lowest Landau level significantly contributes to physical quantities of interest in the high-field limit is lifted by including all the Landau levels. The resulting values in two dimensions are significantly lower than the numerical simulation data of the same model but are in reasonably good quantitative agreement with experimental data on La_2SrCuO_4 above the irreversibility line (below the irreversibility line at which α_{xy} diverges and theory should be modified by including pinning effects). The values of e_N calculated in three dimensions are also in good quantitative agreement with experimental data for temperature close to T_c on $YBa_2Cu_3O_7$. For each of the materials we consider, the melting and the irreversibility lines are also fitted with the same set of parameters using a recent quantitative Ginzburg-Landau theory.

DOI: 10.1103/PhysRevB.79.024518 PACS number(s): 74.40.+k, 74.25.Ha, 74.25.Dw

I. INTRODUCTION

The electric field is induced in a metal under magnetic field by the temperature gradient ∇T perpendicular to the magnetic field **H**, which is a phenomenon known as Nernst effect[1] (direction of the electric field being perpendicular to both ∇T and **H**). Recently the Nernst effect in high-T_c superconductors attracted attention both theoretically[1–6] and experimentally.[7–15] In these materials, effect of thermal fluctuations is very strong leading to depinning of Abrikosov vortices created by the magnetic field in type-II superconductor below second critical field $H_{c2}(T)$. In the mixed state the Nernst effect is large due to vortex motion while in the normal state and in the vortex lattice or glass states, it is typically smaller. The Nernst effect therefore is a probe of thermal fluctuations phenomena in the vortex matter but in principle could shed some light on the underlying microscopic mechanism of superconductivity in cuprates.

The appearance of a fluctuation tail above the critical temperature in the Nernst signal was observed in strongly type-II superconductors, both with low T_c such as $NbSe_2$ and $Nb_{0.15}Si_{0.85}$ films,[15] and several different high-temperature materials.[8–11,14] The related Ettingshausen effect was detected as well.[7] In particular, the Nernst effect was observed well above $T_{c2}(H)$ and even above T_c in $Bi_2Sr_2CaCu_2O_{8+\delta}$ (Ref. 14) (BiSCCO), strongly underdoped $YBa_2Cu_3O_y$ (Refs. 11, 12, and 14) (YBCO), and $La_{2-x}Sr_xCuO_4$ (Refs. 10, 11, 13, and 14) (LaSCO). These layered materials are highly anisotropic and can be described by a quasi-two-dimensional (2D) model. Due to reduced dimensionality the effect of thermal fluctuations is greatly enhanced. However even in less anisotropic materials such as the hole-doped cuprate $Nd_{2-x}Ce_xCuO_4$ (Ref. 14) (NCCO), and weakly anisotropic and overdoped or fully oxidized $YBCO_{6.99}$,[14] the effect persists. Fluctuations in these materials cannot be described by a 2D model and generalization to anisotropic three-dimensional (3D) models is required. Measurements of e_N in fields H up to 45 T (Ref. 14) reveal that the vortex-Nernst signal e_N has a characteristic "tilted-hill" profile, which is qualitatively distinct from that of quasiparticles. The hill profile, which is observed above and below T_c, underscores the continuity between the vortex-liquid state below T_c and the Nernst region above T_c.

Recently, the study of the Nernst effect in $NbSe_2$ reveals a large quasiparticle contribution with a magnitude comparable and a sign opposite to the vortex signal.[15] A large negative Nernst coefficient, persisting at temperatures well above $T_c = 7.2$ K, was found in this metal. The quasiparticle contribution to the Nernst signal attains a magnitude comparable to the vortex signal in the superconducting state. More recently, in experiment on amorphous thin films of the conventional superconductor $Nb_{0.15}Si_{0.85}$,[15] a Nernst signal was generated by short-lived Cooper pairs in the normal state. In these amorphous films, the contribution of free electrons to the Nernst signal is negligible. The extremely short mean-free path of electrons in amorphous $Nb_{0.15}Si_{0.85}$ damps the normal-state Nernst effect and allows a direct comparison of the data with theory. In the zero-field limit and close to T_c, the magnitude of the Nernst coefficient was found to be in quantitative agreement with a theoretical prediction by Ussishkin *et al.*,[3] invoking the superconducting correlation length as its single parameter. At high temperature and finite magnetic field, the data were found to deviate from the theoretical expression. In electron-doped cuprate (NCCO) the quasiparticle contribution to the Nernst signal is large.[14] The quasiparticle contribution actually dominates the Nernst signal far below T_c. Nevertheless, the vortex signal retains its characteristic tilted-hill profile which is easily distinguished from the monotonic quasiparticle contribution.

We will concentrate on the vortex-Nernst effect in type-II superconductor of the overdoped LaSCO,[12] and underdoped and overdoped YBCO,[12] where e_N is intrinsically strongly nonlinear in H and generally much larger than that in nonmagnetic normal metal. The observation of the Nernst effect above T_c along with other strong fluctuation effects was interpreted as a support for the preformed pair scenario for the mechanism of the transition to the superconducting state. At

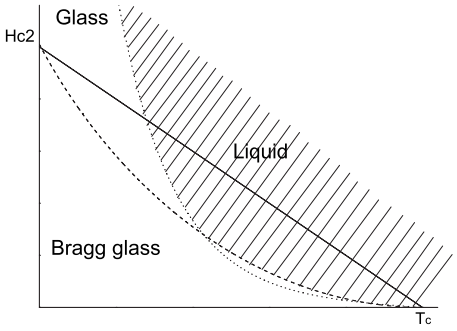

FIG. 1. The thermodynamic phase diagram.

the same time thermal fluctuations in high-T_c materials lead to many other remarkable phenomena, most notably vortex lattice melting and thermal depinning that are well studied both experimentally and theoretically over the last two decades, so that the theory of the Nernst effect should be consistent with the theory of these phenomena. Most importantly, the material parameters determining the fluctuation strengths can be determined from these better studied effects since in many recent experiments at least the melting line was measured on the same samples.

Theory of the electronic and the heat transport (including the Nernst effect) based on the phenomenological time-dependent Ginzburg-Landau (TDGL) equations with thermal noise describing strongly fluctuating superconductors was developed long time ago.[1,2] More recently within the same framework Ussishkin *et al.*[3] calculated perturbatively the low-field Nernst effect for $T>T_c$ due to contribution of Gaussian fluctuations and obtained results in agreement with a microscopic Aslamazov-Larkin[1] calculation. Mukerjee and Huse[5] numerically simulated the two-dimensional TDGL equation with Langevin thermal noise for $T<T_c$ and obtained results in reasonable agreement with experimental data on LaSCO (Ref. 12) at lower temperature but the transverse thermoelectric conductivity became independent of magnetic field at higher temperatures in contrast to experiment. The simulation of this system, even in 2D, is difficult and it was one of our goals to supplement it with a reliable analytical expression in the region of the vortex liquid, namely, in the region above the melting line (see Fig. 1) at which the vortex matter becomes homogeneous on a scale of several lattice spacings and the crystalline symmetry is lost. In this phase the pinning is ineffective and, unlike in the vortex glass phase, vortices actively promote the Nernst effect. Recent understanding of the vortex matter phase diagram is summarized in Fig. 1. There are four phases separated by two transition lines:[16] the first-order melting line (sometimes called the order-disorder line at lower temperatures, dashed line in Fig. 1) and the irreversibility (or glass) continuous transition. The melting line separates crystalline phases from homogeneous phases while the glass line (dotted line in Fig. 1) separates pinned phases from the unpinned ones. The mean-field $H_{c2}(T)$ line (solid line in Fig. 1) in strongly fluctuating superconductors becomes a crossover. Both pinning and crystalline order lead to a strong reduction in the Nernst signal and therefore these phases will not be considered here. We concentrate on the vortex-liquid phase (dashed area in Fig. 1), and discuss the melting line and disorder only as limits of applicability of the theory and for determining the material parameters. The quantitative Ginzburg-Landau (GL) theory of the vortex liquid has been developed recently and it was established that the Hartree-Fock approach for the thermodynamics is close to the convergent Borel-Pade one in the wide region of the vortex-liquid phase.[17]

In this paper we revisit the Hartree-Fock calculation in TDGL originally performed in Ref. 2 to obtain explicit expressions for the transverse thermoelectric conductivity α_{xy} and the Nernst signal e_N in both 2D and 3D. Typically only the lowest Landau level (LLL) contribution was investigated.[18] We extend it to higher Landau levels necessary for exploring the experimentally accessible parameter region and find a range of applicability of the results due to approximations made, disorder, and crystallization. In this theory the strength of the thermal fluctuations is described by just one dimensionless adjustable parameter η (closely related to the Ginzburg number Gi). This parameter determines simultaneously the location of the melting line measured on the same samples in recent experiments on Nernst effect. The expression of Ref. 17 for the melting line is in good agreement with many experiments in very wide range of materials (as was established recently in Ref. 19) and Monte Carlo (MC) simulation. Then fitting of the transverse thermoelectric conductivity and related quantities practically has no free parameters (of course there is a certain freedom in determining mean-field parameters such as H_{c2} and T_c but the range is limited by experimental values). The value fitted from the Nernst effect turns out to be consistent with that derived from the melting line calculated in Ref. 17. We will present the fitting of the melting line for the overdoped LaSCO,[12] and underdoped and overdoped YBCO.[12]

The paper is organized as follows. The model is defined in Sec. II. The transverse thermoelectric conductivity in the vortex-liquid phase and extension to anisotropic 3D model are described in Sec. III. The comparison with experiment and MC simulation data is described in Sec. IV. We conclude in Sec. V. The Appendix calculates magnetization in the vortex liquid within the Gaussian approximation.

II. GINZBURG–LANDAU MODEL IN 2D

A. Relaxation dynamics and thermal fluctuations

To describe fluctuation of order parameter in thin films or layered superconductors, one can start with the Ginzburg-Landau free energy:

$$F = s\int d^2x \frac{\hbar^2}{2m^*}|\mathbf{D}\psi|^2 + a|\psi|^2 + \frac{b'}{2}|\psi|^4, \qquad (1)$$

where $\mathbf{A}=(-By,0)$ describes a constant and practically homogeneous magnetic field (we generally neglect small fluctuations of the magnetic field due to magnetization which are of order $1/\kappa^2 \ll 1$ in the region of interest) in Landau gauge and the covariant derivative is defined by $\mathbf{D}\equiv\nabla - i(2\pi/\Phi_0)\mathbf{A}$, with $\Phi_0=hc/e^*$, $e^*=-2e>0$. For simplicity we assume linear dependence $a(T)=\alpha(T-T^{\Lambda})$ although the

temperature dependence can be easily modified to better describe the experimental coherence length. The "mean-field" critical temperature T^{Λ} depends on the ultraviolet (UV) cutoff Λ specified later. It is higher than measured critical temperature due to strong thermal fluctuations on the mesoscopic scale. The thickness of a layer, s, is assumed to be small enough so that order parameter does not vary considerably inside the layer [namely, does not exceed the coherence length $\xi_z(T)$ along the field direction], and layers are nearly independent. We apply this model to describe experiments not just in BiSCCO and other highly anisotropic materials but also in overdoped LaSCO (Ref. 12) and strongly underdoped YBCO.[12] For more isotropic optimally doped or fully doped YBCO (Ref. 12), an anisotropic 3D GL model (neglecting the layered structure) would be more appropriate. For materials between the two extremes, a more complicated model such as the Lawrence-Doniach one should be used.

Since we are interested in transport phenomena, it is necessary to introduce some kind of dynamics for the order parameter. The simplest is a gauge-invariant version of the "type A" relaxational dynamics,

$$\tau\left(\frac{\partial}{\partial t}+i\frac{e^*}{\hbar}\phi\right)\psi=-\frac{\delta F}{\delta\psi^*}+\zeta, \tag{2}$$

called in the present context TDGL equation. Explicitly the TDGL equation for the superconducting order parameter is

$$\tau\left(\frac{\partial}{\partial t}+i\frac{e^*}{\hbar}\phi\right)\psi=\frac{\hbar^2}{2m^*}\mathbf{D}^2\psi-a\psi-b'|\psi|^2\psi+\zeta, \tag{3}$$

where $\phi(\mathbf{x})$ is the scalar potential describing electric field. To incorporate the thermal fluctuations via Langevin method, the noise term $\zeta(\mathbf{x},t)$ having Gaussian correlations,

$$s\langle\zeta^*(\mathbf{x},t)\zeta(\mathbf{x}',t')\rangle=2T\tau\delta(\mathbf{x}-\mathbf{x}')\delta(t-t'), \tag{4}$$

is introduced. Here $\delta(\mathbf{x}-\mathbf{x}')$ is the two-dimensional δ function of the in-plane coordinates, and the relaxation-time rate τ in the TDGL equation is given by[20]

$$\tau=\frac{\pi\hbar^3}{16m^*\xi^2T}. \tag{5}$$

B. Heat and the electric transport

The total heat current density in GL model reads

$$\mathbf{j}^h=-\frac{\hbar^2}{2m^*}\left\langle\left(\frac{\partial}{\partial t}-i\frac{e^*}{\hbar}\phi\right)\Psi^*\left(\nabla-i\frac{2\pi}{\Phi_0}\mathbf{A}\right)\Psi\right\rangle+\text{c.c.}, \tag{6}$$

while the total electric current is

$$\mathbf{j}^e=-i\frac{e^*\hbar}{2m^*}\left\langle\Psi^*\left(\nabla-i\frac{2\pi}{\Phi_0}\mathbf{A}\right)\Psi\right\rangle+\text{c.c.} \tag{7}$$

An important aspect of the calculation of the electrothermal conductivity, discussed in detail,[21] is the need to account for the magnetization currents. In the presence of magnetic field, a system has the magnetization current in equilibrium. The total heat current defined in Eq. (6) is thus a sum of the transport and the magnetization parts,

$$\mathbf{j}^h=\mathbf{j}^h_{\text{tr}}+\mathbf{j}^h_{\text{mag}}. \tag{8}$$

In the presence of an applied electric field, it was shown in Ref. 21 that the magnetization current is given by

$$\mathbf{j}^h_{\text{mag}}=c\mathbf{M}\times\mathbf{E}, \tag{9}$$

where $\mathbf{M}$ is the equilibrium magnetization.

Generally, to define the transport coefficients, the electric and heat *transport* current densities, $\mathbf{j}^{(e)}$ and $\mathbf{j}^{(h)}$, in metal are related to the applied (sufficiently weak) electric field and the temperature gradient by

$$j^{(e)i}_{\text{tr}}=\sigma^{ij}E^j-\alpha^{ij}\nabla^jT, \tag{10}$$

$$j^{(h)i}_{\text{tr}}=\tilde{\alpha}^{ij}E^j-\kappa^{ij}\nabla^jT, \tag{11}$$

where σ, α, $\tilde{\alpha}$, and κ are the electrical, the thermoelectric, the electrothermal, and the thermal-conductivity components of the conductivity tensor $(i,j=x,y)$. The Onsager relation implies $\tilde{\alpha}=T\alpha$. The Nernst coefficient ν_N, under the condition $\mathbf{j}^{(e)}_{\text{tr}}=0$, is expressed in terms of the above coefficients as

$$\nu_N=\frac{E_y}{(-\nabla T)_xB}=\frac{1}{B}\frac{\alpha_{xy}\sigma_{xx}-\alpha_{xx}\sigma_{xy}}{\sigma_{xx}^2+\sigma_{xy}^2}. \tag{12}$$

If the system shows no significant Hall effect (only such systems will be considered), then $\sigma_{xy}=0$ and the expression simplifies:

$$\nu_N=\frac{\alpha_{xy}}{B\sigma_{xx}}. \tag{13}$$

The Nernst signal is defined

$$e_N=\frac{E_y}{(-\nabla T)_x}=B\nu_N. \tag{14}$$

For comparison with experiment, the fluctuation contribution, σ_{xx} and e_N, should be added to the normal-state contribution, σ^n and e^n_N. However, in the normal state the Nernst signal e^n_N is very small in these materials[3,14] and will be largely ignored in what follows.

It then follows that the electrothermal conductivity is given by

$$\tilde{\alpha}_{xy}\equiv\frac{j^h_{(\text{tr})x}}{E_y}=\frac{j^h_x}{E_y}+cM_z. \tag{15}$$

Both terms contribute as will be shown in the following sections.

III. TRANSVERSE THERMOELECTRIC CONDUCTIVITY IN THE VORTEX-LIQUID PHASE

A. Melting of the vortex solid, vortex glass, and the range of validity of the Gaussian approximation

At low temperatures vortex matter organizes itself into a (usually, but not always) hexagonal vortex lattice. When disorder can be effectively neglected (either in very clean materials or when thermal depinning occurs), one can consider transport of the vortex lattice as a whole. Expressions for the

electric and the thermal conductivities near $H_{c2}(T)$ that neglect thermal fluctuations were obtained in Ref. 2, and according to results the Nernst effect is generally very small compared to one in the vortex liquid. This can be qualitatively understood as a result of rigidity of the lattice. *Below* the melting line the situation in this respect does not change much. Moreover due to unavoidable presence of disorder, the vortex lattice is pinned forming a Bragg glass in most of its domain.[16] However in high-T_c superconductors thermal fluctuations are strong enough (especially for high anisotropy and high magnetic fields) to destroy the expectation value of the condensate $\langle\psi\rangle=0$. We always assume that thermal fluctuations melted away and in addition temperature is high enough to thermally depin the vortex liquid (avoiding the "vortex glass"). As a consequence impurities in the vortex liquid are neutralized. To determine the range of validity of the above assumptions, one has to estimate the location of the melting and the irreversibility lines. Within the LLL approximation (which is valid *near melting* in wide range of parameters[17]), the line separating the crystalline and the homogeneous phases is given in 2D by

$$a_T^{2D} \equiv -(2\mathrm{Gi}_{2D})^{-1/4}(\pi bt)^{-1/2}(1-t-b) = -13.6, \quad (16)$$

where a_T is the dimensionless "LLL scaled" temperature with

$$\mathrm{Gi}_{2D} \equiv \frac{1}{2}\left(\frac{8e^2\kappa^2\xi^2 T_c}{\pi c^2\hbar^2 s}\right)^2, \quad (17)$$

being a 2D analog of the Ginzburg parameter characterizing the strength of thermal fluctuations on the mesoscopic scale. Scaled magnetic field is $b=B/H_{c2}(0)$ with $H_{c2}(0)=\Phi_0/2\pi\xi^2$ being the zero-temperature critical field (extrapolated by the linear formula from T_c, actual $H_{c2}(T)$ at $T=0$ is lower), $\xi=(\hbar^2/2m^*\alpha T_c)^{1/2}$ being the zero-temperature correlation length, and $t=T/T_c$. Equation (16) determines the melting line in Fig. 1 and in turn the melting line fixes the Gi in all the fits to experimental data below. This expression was obtained from the comparison of the calculated free energies of the vortex lattice (expansion to two loop order) and of the vortex liquid within the Borel-Pade approach. The corresponding value and definition for 3D are

$$a_T^{3D} = -2^{1/3}(\mathrm{Gi}_{3D})^{-1/3}(\pi bt)^{-2/3}(1-t-b) = -9.5, \quad (18)$$

where

$$\mathrm{Gi}_{3D} \equiv \frac{1}{2}\left(\frac{8e^2\kappa^2\xi T_c\gamma}{\pi c^2\hbar^2}\right)^2, \quad (19)$$

and $\gamma\equiv\sqrt{m_c/m^*}$ is an anisotropy parameter.

In the presence of disorder, vortex matter can be pinned. It leads to several phenomena. On the one hand the vortex lattice is destroyed effectively at large fields but on the other hand vortices are pinned and cannot take advantage of thermal fluctuations. The irreversibility or the vortex glass line determining the region in which thermal fluctuations overpower the quench by disorder is given in 2D by[16,22]

$$a_T^g \equiv 4\frac{2r-1}{\sqrt{2r}}, \quad (20)$$

where

$$r = \frac{\mathrm{Gi}_{2D}^{-1/2}}{4t}(1-t)^2 n, \quad (21)$$

and dimensionless parameter n characterizes the disorder strength.[17] This determines the dotted line in Fig. 1.

B. Vortex liquid within the Gaussian approximation

Due to thermal fluctuations the expectation value of the order parameter in vortex liquid is zero $\langle\psi(\mathbf{x},t)\rangle=0$. Therefore contribution to the expectation values of physical quantities such as the electric and the heat currents come exclusively from the correlations. The most important is the quadratic one,

$$C(\mathbf{x},t;\mathbf{x}',t') = \langle\psi(\mathbf{x},t)\psi^*(\mathbf{x}',t')\rangle, \quad (22)$$

called the correlation function of the order parameter. In particular the superfluid density is

$$\langle|\psi(\mathbf{x},t)|^2\rangle = C(\mathbf{x},t;\mathbf{x},t). \quad (23)$$

A simple approximation which captures the most interesting fluctuation effects in the Gaussian approximation (see Ref. 23 for details), in which the cubic term in the GL equation Eq. (3) $b'|\psi|^2\psi$ is replaced by a linear one $2b'\langle|\psi|^2\rangle\psi$:

$$\tau\frac{\partial}{\partial t}\psi(\mathbf{x},t) = \left(\frac{\hbar^2}{2m^*}\mathbf{D}^2 - \tilde{a}\right)\psi(\mathbf{x},t) + \zeta(\mathbf{x},t), \quad (24)$$

leading the "renormalized" value of the coefficient:

$$\tilde{a} = a + 2b'\langle|\psi|^2\rangle. \quad (25)$$

The formal solution of this equation is

$$\psi(\mathbf{x},t) = \int d\mathbf{x}'\int dt' G_0(\mathbf{x},t;\mathbf{x}',t')\zeta(\mathbf{x}',t'), \quad (26)$$

where G_0 is the equilibrium Green's function.

In the Landau gauge, one has

$$G_0(\mathbf{x},t;\mathbf{x}',t') = \frac{1}{4\pi^2}\left(\frac{m^*\omega_B}{\hbar}\right)^{1/2}\int_{\omega,\tilde{y}_0} G_0(\tilde{y},\tilde{y}',\omega,\tilde{y}_0) \times e^{-i(m^*\omega_B/\hbar)^{1/2}\tilde{y}_0(x-x')}e^{i\omega(t-t')}, \quad (27)$$

where $\tilde{y}=(m^*\omega_B/\hbar)^{1/2}y$ with $\omega_B=e^*B/m^*c$, and $\tilde{y}_0=-(\hbar/m^*\omega_B)^{1/2}k_x$, with k_x as the x component of the vector momentum and

$$G_0(\tilde{y},\tilde{y}',\omega,\tilde{y}_0) = \left(\frac{m^*\omega_B}{\hbar\pi}\right)^{1/2}\exp[-(\tilde{y}-\tilde{y}_0)^2/2 - (\tilde{y}'-\tilde{y}_0)^2/2]\sum_n \frac{1}{2^n n!}\frac{H_n(\tilde{y}-\tilde{y}_0)H_n(\tilde{y}'-\tilde{y}_0)}{(i\tau\omega+E_n)}, \quad (28)$$

with the energy eigenvalues,

$$E_n = \left(n + \frac{1}{2}\right)\hbar\omega_B + \tilde{a}, \tag{29}$$

(H_n are the Hermite polynomials). Averaging over the noise, Eqs. (4) and (26), the equilibrium correlation function [Eq. (22)] is

$$C_0(\mathbf{x},t;\mathbf{x}',t') = \frac{2\tau T}{s}\int_{\mathbf{x}_1,t_1} G_0(\mathbf{x},t;\mathbf{x}_1,t_1)G_0^*(\mathbf{x}',t';\mathbf{x}_1,t_1)$$
$$= -\frac{T}{2\pi^2 s}\left(\frac{m^*\omega_B}{\hbar}\right)^{1/2}\int_{\omega,\tilde{y}_0}\frac{ImG_0(\tilde{y},\tilde{y}',\omega,\tilde{y}_0)}{\omega}$$
$$\times e^{-i(m^*\omega_B/\hbar)^{1/2}\tilde{y}_0(x-x')}e^{i\omega(t-t')}, \tag{30}$$

which enters the self-consistent equation (sometimes called gap equation) [Eq. (25)], determining $\tilde{a}$. In equilibrium, $\langle|\psi(\mathbf{x},t)|^2\rangle$ is

$$\langle|\psi(\mathbf{x},t)|^2\rangle = \frac{T}{2\pi s}\frac{m^*\omega_B}{\hbar}\sum_n \frac{1}{E_n}. \tag{31}$$

Thus Eq. (25) becomes

$$\epsilon_b = \tilde{\epsilon}_b - \frac{b'T}{\pi s}\frac{m^*\omega_B}{\hbar(\alpha T^\Lambda)^2}\sum_{n=0}^{N_f}\frac{1}{\tilde{\epsilon}_b + 2nb}, \tag{32}$$

where the reduced temperature is defined as $\epsilon = a/\alpha T^\Lambda$, $\epsilon_b = \epsilon + b$ (with similar expression for $\tilde{\epsilon}$ and $\tilde{\epsilon}_b$). The UV cutoff Λ was introduced. It effectively limits the number of Landau levels to $N_f = \frac{\Lambda}{b} - 1$. The "bubble" sum, which diverges logarithmically, can be performed as

$$\frac{b}{\pi}\sum_{n=0}^{N_f}\frac{1}{2nb + \tilde{\epsilon}_b} = \frac{1}{2\pi}\log\Lambda + u', \tag{33}$$

where the function u' is related by

$$u'(\tilde{\epsilon}_b, b) = \frac{1}{2\pi}[f_s'(\tilde{\epsilon}_b/2b) - \log(2b)], \tag{34}$$

to the polygamma function f_s':

$$f_s'(x) = \sum_{n=1}^{\infty}\left[\frac{1}{n+x} - \int_{n-1/2}^{n+1/2}\frac{1}{(y+x)}dy\right] + \left[\frac{1}{x} - \log(x+1/2)\right]. \tag{35}$$

Thus the critical temperature T_c is significantly renormalized:

$$\epsilon_b^r = \epsilon_b + \frac{b'T}{2\pi s}\frac{m^*\omega_B}{\hbar(\alpha T^\Lambda)^2}\log\Lambda = \tilde{\epsilon}_b - \eta u'(\tilde{\epsilon}_b, b), \tag{36}$$

where η is a dimensionless fluctuation parameter

$$\eta = \frac{b'T_c}{\xi^2(\alpha T_c)^2 s}, \tag{37}$$

introduced in Ref. 5. The relation between η used to describe thermal transport and the more often used two-dimensional Ginzburg number[1,17] Gi_{2D}, see Eq. (17), is

$$\eta = 4\sqrt{2\mathrm{Gi}_{2D}}\pi^2. \tag{38}$$

C. Expectation value of the heat current in linear response to electric field

Let us assume that the weak electric field $\mathbf{E}$ is along the y axis, generated by the scalar potential $\phi = -E_y y$. The heat and the electric currents in the vortex-liquid phase can be written as

$$\mathbf{j}^h = -\frac{\hbar^2}{2m^*}\left[\mathbf{D}(\mathbf{x})\left(\frac{\partial}{\partial t'} - i\frac{e^*}{\hbar}\phi(\mathbf{x}')\right) + \mathbf{D}^*(\mathbf{x}')\left(\frac{\partial}{\partial t} + i\frac{e^*}{\hbar}\phi(\mathbf{x})\right)\right]C(\mathbf{x},t;\mathbf{x}',t')|_{\mathbf{x}=\mathbf{x}';t=t'}, \tag{39}$$

$$\mathbf{j}^e = \left[\frac{\hbar e^*}{2m^* i}(\nabla - \nabla') - \frac{e^{*2}}{2m^* c}\mathbf{A}(x)\right]C(\mathbf{x},t;\mathbf{x}',t')|_{\mathbf{x}=\mathbf{x}';t=t'}, \tag{40}$$

where

$$C(\mathbf{x},t;\mathbf{x}',t') = \frac{2\tau T}{s}\int_{\mathbf{x}_1,t_1} G(\mathbf{x},t;\mathbf{x}_1,t_1)G^*(\mathbf{x}',t';\mathbf{x}_1,t_1), \tag{41}$$

with G as the Green's function of the linearized TDGL equation in the presence of the scalar potential. One finds correction to the Green's function to linear order in the electric field

$$G(\mathbf{x},t;\mathbf{x}',t') = G_0(\mathbf{x},t;\mathbf{x}',t') - i\frac{e^*\tau}{\hbar}\int_{\mathbf{x}_1,t_1}\phi(\mathbf{x}_1)$$
$$\times G_0(\mathbf{x},t;\mathbf{x}_1,t_1)G_0(\mathbf{x}_1,t_1;\mathbf{x}',t'). \tag{42}$$

The transverse thermoelectric conductivity is obtained by expanding the correlation function to linear order in the electric field. The correlation function C in terms of the Green's function G_0 using Eqs. (30), (41), and (42) takes the form

$$C(\mathbf{x},t;\mathbf{x}',t') = C_0(\mathbf{x},t;\mathbf{x}',t') + C_1(\mathbf{x},t;\mathbf{x}',t'), \tag{43}$$

where

$$C_1(\mathbf{x},t;\mathbf{x}',t') = i\frac{e^*\tau}{\hbar}\int_{\mathbf{x}_1,t_1}\phi(\mathbf{x}_1)[G_0^*(\mathbf{x}',t';\mathbf{x}_1,t_1)C_0(\mathbf{x},t;\mathbf{x}_1,t_1)$$
$$- G_0(\mathbf{x},t;\mathbf{x}_1,t_1)C_0^*(\mathbf{x}',t';\mathbf{x}_1,t_1)]$$
$$= i\frac{e^*\tau T E_y}{2\pi^2\hbar s}\left(\frac{\hbar}{m^*\omega_B}\right)^{1/2}\int\frac{d\omega}{\omega}$$
$$\times\int_{\tilde{y}_0,\tilde{y}_1}\tilde{y}_1[G_0^*(\tilde{y}',\tilde{y}_1,\omega,\tilde{y}_0)$$
$$\times ImG_0(\tilde{y},\tilde{y}_1,\omega,\tilde{y}_0) - G_0(\tilde{y},\tilde{y}_1,\omega,\tilde{y}_0)$$
$$\times ImG_0(\tilde{y}',\tilde{y}_1,\omega,\tilde{y}_0)]$$
$$\times e^{-i(m^*\omega_B/\hbar)^{1/2}\tilde{y}_0(x-x')}e^{i\omega(t-t')}. \tag{44}$$

In order to determine the transverse thermoelectric conductivity, we need to compute the x component of the heat current to the first order in the electric field. In the chosen gauge, the heat current along the x direction under condition

$j_{\rm tr}^{e(x)}=0$ also contains two terms. The term coming from C_0 vanishes,

$$j_0^{(h)x}=\frac{\hbar T\omega_B}{2\pi^2 s}\int_{\omega,\tilde{y}_0}(\tilde{y}-\tilde{y}_0)ImG_0(\tilde{y},\omega,\tilde{y}_0)=0, \quad (45)$$

because $ImG_0(\tilde{y},\omega,\tilde{y}_0)$ is an odd function of ω. It is possible to interpret easily that C_0 is the equilibrium correlation function which does not contribute to the current. Considering C_1,

$$\begin{aligned} j_1^{(h)x}&=\frac{2e^{*2}E_y\tau^3BT}{\pi^2 m^* cs}\sum_{nm}\frac{1}{2^n n!}\frac{1}{2^m m!}\int_{-\infty}^{+\infty}\frac{d\omega}{2\pi}\omega^2 \\ &\times\frac{1}{(E_n^2+\tau^2\omega^2)}\frac{1}{(E_m^2+\tau^2\omega^2)}\int_{-\infty}^{+\infty}d\tilde{y}_0\int_{-\infty}^{+\infty}d\tilde{y}_1\tilde{y}_1(\tilde{y}_0-\tilde{y}) \\ &\times\exp[-(\tilde{y}-\tilde{y}_0)^2-(\tilde{y}_1-\tilde{y}_0)^2]H_n(\tilde{y}-\tilde{y}_0)H_n(\tilde{y}_1 \\ &-\tilde{y}_0)H_m(\tilde{y}-\tilde{y}_0)H_m(\tilde{y}_1-\tilde{y}_0) \\ &=\frac{e^*E_yT(b-\tilde{\epsilon}_b)}{2\hbar bs}[u'(\tilde{\epsilon}_b,b)-u'(\tilde{\epsilon}_b+b,b)]. \end{aligned} \quad (46)$$

In order to calculate the transport coefficient α_{xy} using the Onsager relation [Eq. (15)], we need the equilibrium magnetization. This is calculated in the Appendix with the result given in Eq. (A10). Together with Eq. (46) one obtains the transverse thermoelectric conductivity

$$\begin{aligned} \alpha_{xy}\equiv\frac{\tilde{\alpha}_{xy}}{T}&=\frac{e^*}{2\hbar\pi bs}[\pi(b-\tilde{\epsilon}_b)u'(\tilde{\epsilon}_b,b)-\pi(b-\tilde{\epsilon}_b)u'(\tilde{\epsilon}_b \\ &+b,b)-\partial_b u(\tilde{\epsilon}_b,b)+\eta tu'\partial_b u']. \end{aligned} \quad (47)$$

Analogous calculation of the electrical conductivity $\sigma_{yy}=\frac{\overline{j_y^e}}{E_y}$ (averaged over $\mathbf{x}$) results in

$$\begin{aligned} \sigma_{yy}&=\frac{e^{*2}}{16s\hbar}\sum_n(n+1)\left(\frac{1}{2nb+\tilde{\epsilon}_b}+\frac{1}{2(n+1)b+\tilde{\epsilon}_b}\right. \\ &\left.-\frac{2}{2(n+1/2)b+\tilde{\epsilon}_b}\right) \\ &=\frac{\pi e^{*2}}{32s\hbar b^2}[(2b-\tilde{\epsilon}_b)u'(\tilde{\epsilon}_b,b)-\tilde{\epsilon}_b u'(\tilde{\epsilon}_b+2b,b) \\ &-2(b-\tilde{\epsilon}_b)u'(\tilde{\epsilon}_b+b,b)]. \end{aligned} \quad (48)$$

D. Extension to anisotropic 3D model

For 3D materials with asymmetry along the z axis, the GL model takes the form

$$F=\int d^3x\frac{\hbar^2}{2m^*}|\mathbf{D}\psi|^2+\frac{\hbar^2}{2m_c}|\partial_z\psi|^2+a|\psi|^2+\frac{b'}{2}|\psi|^4. \quad (49)$$

The TDGL equation for the superconducting order parameter in the Gaussian approximation is now

$$\tau\left(\frac{\partial}{\partial t}+i\frac{e^*}{\hbar}\phi\right)\psi=\left(\frac{\hbar^2}{2m^*}\mathbf{D}^2+\frac{\hbar^2}{2m_c}\partial_z^2-\tilde{a}\right)\psi+\zeta. \quad (50)$$

The gap equation can be written as

$$\epsilon_b^r=\tilde{\epsilon}_b-\eta_{3D}tu'_{3D}, \quad (51)$$

where $u'_{3D}=\partial u_{3D}/\partial\tilde{\epsilon}_b$. The function u_{3D} can be written in the following form:

$$u_{3D}(\tilde{\epsilon}_b,b)=\frac{1}{\sqrt{2}\pi}b^{3/2}v\left(\frac{\tilde{\epsilon}_b}{2b}\right), \quad (52)$$

with

$$\begin{aligned} v(x)=\sum_{n=0}^{\infty}&\left[\sqrt{n+x}-\frac{2}{3}\left(x+n+\frac{1}{2}\right)^{3/2}+\frac{2}{3}\left(x+n-\frac{1}{2}\right)^{3/2}\right] \\ &-\frac{2}{3}\left(x-\frac{1}{2}\right)^{3/2}. \end{aligned} \quad (53)$$

The dimensionless fluctuation parameter η_{3D} is

$$\eta_{3D}=\frac{b'T_c}{\xi^2(\alpha T_c)^2\xi_z}, \quad (54)$$

with $\xi_z=(\hbar^2/2m_c\alpha T_c)^{1/2}$ as the zero-temperature correlation length along the field direction.

The relation between η_{3D} used to describe thermal transport in this case and three-dimensional Ginzburg number[1,17] Gi_{3D}, see Eq. (19), is

$$\eta_{3D}=4\sqrt{2\mathrm{Gi}_{3D}}\pi^2. \quad (55)$$

The transverse thermoelectric conductivity is

$$\begin{aligned} \alpha_{xy}&=\frac{e^*}{2\pi\hbar\xi_z b}[\pi u_{3D}(\tilde{\epsilon}_b,b)-\pi u_{3D}(\tilde{\epsilon}_b+b,b) \\ &+\pi(b-\tilde{\epsilon}_b)u'_{3D}(\tilde{\epsilon}_b,b)-\pi(b-\tilde{\epsilon}_b)u'_{3D}(\tilde{\epsilon}_b+b,b) \\ &-\partial_b u_{3D}+\eta_{3D}tu'_{3D}\partial_b u'_{3D}], \end{aligned} \quad (56)$$

while the electrical conductivity

$$\begin{aligned} \sigma_{yy}&=\frac{\pi e^{*2}}{32\xi_z\hbar b^2}[u_{3D}(\tilde{\epsilon}_b,b)+u_{3D}(\tilde{\epsilon}_b+b,b) \\ &-2u_{3D}(\tilde{\epsilon}_b+b,b)+2(b-\tilde{\epsilon}_b)u'_{3D}(\tilde{\epsilon}_b,b) \\ &-2\tilde{\epsilon}_b u'_{3D}(\tilde{\epsilon}_b+b,b)-2(b-\tilde{\epsilon}_b)u'_{3D}(\tilde{\epsilon}_b+b,b)]. \end{aligned} \quad (57)$$

IV. COMPARISON WITH EXPERIMENT AND MC SIMULATION

Here we compare the results to 2D simulation results of Mukerjee and Huse[5] and several recent experiments on high-T_c cuprates.

A. Two-dimensional thermal fluctuations: LaSCO

The experiment results of Wang *et al.*[12] were obtained from the Nernst effect and resistivity measurements on an overdoped LaSCO sample with $x=0.2$ and $T_c=28$ K. The comparison is presented in Fig. 2 [low temperatures in (a) and close to T_c in (b)]. The parameters used in the calculation are (see definitions above) $H_{c2}(0)=45$ T (thus $\xi=27$ Å) and

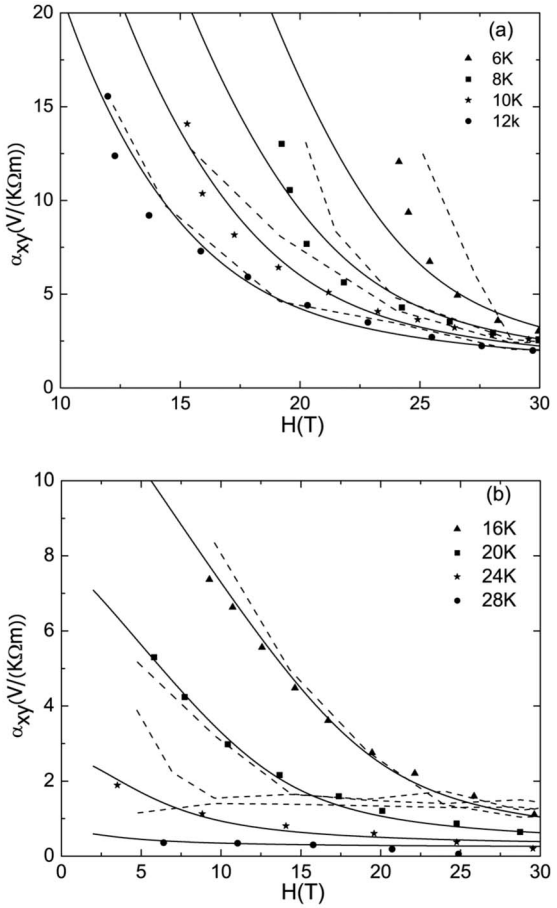

FIG. 2. Points are α_{xy} for different temperatures of LaSCO in Ref. 12, with $x=0.2$ (overdoped, $T_c=28$ K). The dashed line is the simulation value of α_{xy} in Ref. 5. The solid line is the theoretical value of α_{xy}, using $H_{c2}(0)=45$ T, $s=12$ Å, and $\eta=0.18$.

layer spacing $s=12$ Å. The fluctuation parameter is $\eta=0.18$ and provides a reasonable quantitative agreement between theory and experiment. Below the irreversibility line, where the theory should be modified, both pinning and crystalline phase are included in Fig. 2(a). The deviation develops roughly at the location of the irreversibility line. However, our results are in good quantitative agreement with experimental data for temperature close to T_c in Fig. 2(b), where the numerical simulation gives a nearly constant α_{xy}, while the experiment shows more variation.

In Fig. 3 the melting line of overdoped LaSCO of Ref. 12 is fitted using $\mathrm{Gi}_{2D}=1.41\times10^{-5}$, corresponding to $\eta\cong0.21$ which is consistent with the adjusted value of η when we fit the transverse thermoelectric conductivity. The glass (irreversibility) line is estimated from Fig. 2(a), where values of α_{xy} are lower than simulation and experiment data.

B. Two-dimensional thermal fluctuations: underdoped YBCO

We also compared the results to the experiment on an underdoped YBCO sample with $y=6.5$ and $T_c=50$ K in Ref. 12. The parameters used in the calculation are $H_{c2}(0)=72$ T (thus $\xi=22.51$ Å), $s=9$ Å, and the normal-state conductivity $\sigma_n=7.14\times10^5$ $(\Omega\mathrm{m})^{-1}$ in Ref. 24. The fluctuation parameter in this case is fitted to be $\eta=0.51$. Our values are in good quantitative agreement with experimental data for temperature close to T_c in Fig. 4. We find that the theoretical value of e_N has a characteristic "tilted-hill" profile observed in experiment.[11,12,14] In Fig. 5 we present the fitting of the melting line for underdoped YBCO in Ref. 12 that gives $\mathrm{Gi}_{2D}=1.15\times10^{-4}$ and $\eta\cong0.59$, which is consistent with the adjusted value of η when we fit the Nernst signal e_N.

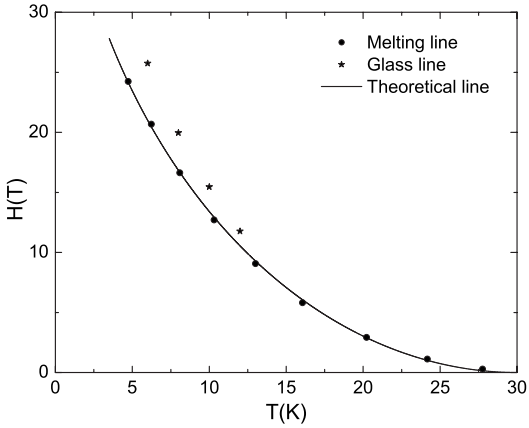

FIG. 3. Comparison of the experimental melting line for overdoped LaSCO in Ref. 12 with our fitting.

C. Three-dimensional thermal fluctuations: overdoped YBCO

We also used the results calculated in three dimensions to compare to the experiment on an overdoped YBCO sample with $y=6.99$ and $T_c=93$ K in Ref. 12. The parameters used in the calculation are $H_{c2}(0)=350$ T (thus $\xi=9.70$ Å), $\xi_z=1.4$ Å, and the normal-state conductivity $\sigma_n=9.45\times10^5$ $(\Omega\mathrm{m})^{-1}$ in Ref. 24. The fluctuation parameter in this case is fitted to be $\eta_{3D}=1.79$. Our values are also in good quantitative agreement with experimental data for temperature close to T_c in Fig. 6. In Fig. 7 we also present the fitting

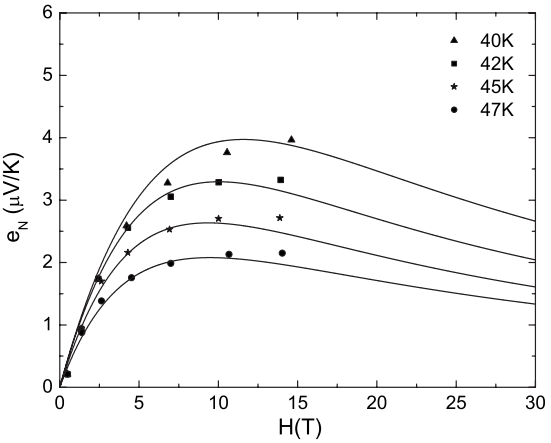

FIG. 4. Points are e_N for different temperatures of YBCO in Ref. 12, with $y=6.5$ (underdoped, $T_c=50$ K). The solid line is the theoretical value of e_N, using $H_{c2}(0)=72$ T, $s=9$ Å, $\sigma_n=7.14\times10^5$ $(\Omega\mathrm{m})^{-1}$, and $\eta=0.51$.

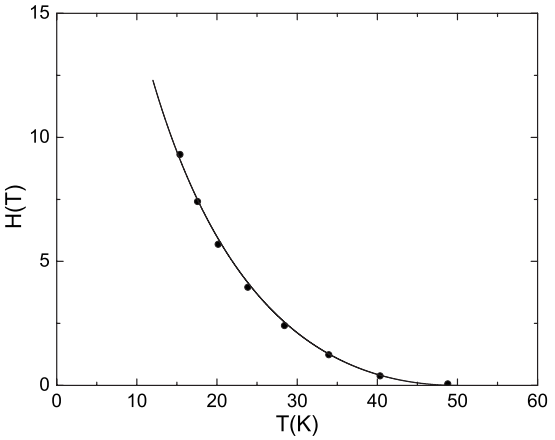

FIG. 5. Comparison of the experimental melting line for underdoped YBCO in Ref. 12 with our fitting.

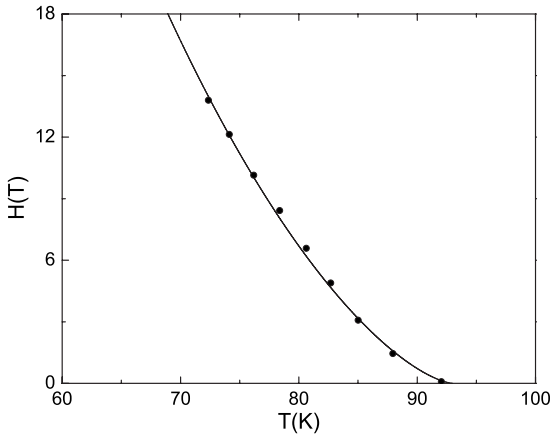

FIG. 7. Comparison of the experimental melting line for overdoped YBCO in Ref. 12 with our fitting.

of the melting line for overdoped YBCO in Ref. 12 that gives $\mathrm{Gi}_{3D}=0.001$ and $\eta_{3D}\cong 2.09$, which is also consistent with the adjusted value of η_{3D} when we fit the Nernst signal e_N.

V. CONCLUSION

Time-dependent Ginzburg-Landau equations with thermal noise describing strong thermal fluctuations on the mesoscopic scale are used to describe strongly type-II superconductor in the vortex-liquid regime both in 2D (describing strongly layered high-T_c superconductors) and 3D (less layered superconductors such as optimally doped YBaCuO). Using GL theory developed earlier, we estimated the region in the parameter space in which, on one hand, vortex crystal is effectively destroyed by thermal fluctuations and, on the other hand, disorder (significantly "weakened" by thermal fluctuations) is not strong enough to significantly affect the transport. Under these conditions we obtained explicit expressions for the transverse thermoelectric conductivity α_{xy} and the Nernst signal e_N including all Landau levels were obtained using a Gaussian approximation. It is very similar to the Hartree-Fock approximation utilized in Ref. 2 but has a virtue of being a variational principle.

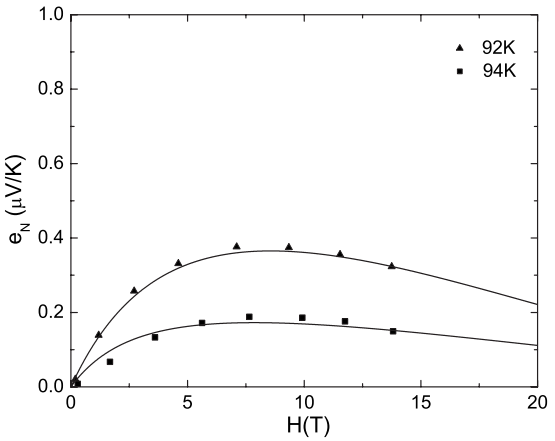

FIG. 6. Points are e_N for different temperatures of YBCO in Ref. 12, with $y=6.99$ (overdoped, $T_c=93$ K). The solid line is the theoretical value of e_N, using $H_{c2}(0)=350$ T, $\xi_z=1.4$ Å, $\sigma_n=9.45\times 10^5$ $(\Omega\mathrm{m})^{-1}$, and $\eta_{3D}=1.79$.

The results are presented using both the strength of the thermal fluctuation η, and the more often used Ginzburg number Gi in the 2D and 3D. The applicability region considered coincides with domain on the phase diagram in which the signal is large. We compared the results to the available 2D numerical simulations of the same model and the experiments on high-T_c materials. Our results in 2D are significantly lower than the available numerical simulation in Ref. 5 below the irreversibility line at which theory should be modified by including both pinning and crystalline correlation effects. However within the applicability region theory is in good qualitative and even quantitative agreement with experimental data on both La_2SrCuO_4 and underdoped $YBa_2Cu_3O_{6.5}$ for temperatures close to T_c.

We also compared the values of e_N calculated in three dimensions with experiment data for temperature close to T_c on $YBa_2Cu_3O_7$, and this comparison is also in good quantitative agreement. The Ginzburg numbers Gi were taken out from the fitting of melting lines of La_2SrCuO_4, $YBa_2Cu_3O_{6.5}$, and $YBa_2Cu_3O_7$ on the same samples. The Ginzburg numbers Gi are consistent with the adjusted values of η when we fit the transverse thermoelectric conductivity and the Nernst signal. The irreversibility line of La_2SrCuO_4 was fitted as well with the same set of parameters.

ACKNOWLEDGMENTS

We are grateful to A. Varlamov for enlightening discussions and encouragement, to Y. Wang for proving the experiment data, to S. Mukerjee for proving the simulation data, to our colleagues J. Y. Juang and C. W. Luo for the valuable discussions, and to A. T. Dorsey for the correspondence. This work was supported by NSC of R. O. C. Contract No. 952112M009048 and MOE ATU program.

APPENDIX: MAGNETIZATION IN THE VORTEX LIQUID WITHIN THE GAUSSIAN APPROXIMATION

In order to calculate magnetization, it is simpler to use the statistical mechanics rather than the (equivalent) time-

dependent Langevin approach. We use the coherence length, ξ, as a unit of length, and $H_{c2}=\Phi_0/2\pi\xi^2$ as a unit of magnetic field. After the order-parameter field is rescaled as $\Psi^2 \rightarrow (2\alpha T_c/b')\psi^2$, the Boltzmann factor can be written as

$$f=\frac{F}{T}=\frac{2}{\eta t}\int d^2x[|D\psi|^2+(\epsilon_b-b)|\psi|^2+|\psi|^4], \quad \text{(A1)}$$

where the dimensionless covariant derivatives are $D=\nabla-iA$. In the framework of the variational Gaussian approximation, the free energy [Eq. (A1)] is divided into an optimized quadratic part K, and a "small" part V. Then K is chosen in such a way that the energy of a Gaussian state is minimal.[17] In liquid phase with an arbitrary homogeneous $U(1)$ symmetric state, just one variational parameter $\tilde{\epsilon}_b$ is sufficient. Thus

$$K=\frac{2}{\eta t}\int d^2x[\psi^*(-D^2-b+\tilde{\epsilon}_b)\psi], \quad \text{(A2)}$$

and the small perturbation becomes

$$V=\frac{2}{\eta t}\int d^2x\left[(\epsilon_b-\tilde{\epsilon}_b)|\psi|^2+\frac{1}{2}|\psi|^4\right]. \quad \text{(A3)}$$

The Gaussian energy which will be minimized therefore is

$$\begin{aligned} f_{\text{gauss}} &\equiv -\log\left[\int D\psi D\bar{\psi}\exp(-K)\right]+\langle V\rangle_K \\ &= \frac{b}{\pi}\sum_{n=0}^{\infty}\log(2nb+\tilde{\epsilon}_b)+(\epsilon_b-\tilde{\epsilon}_b)\frac{b}{\pi}\sum_{n=0}^{\infty}\frac{1}{2nb+\tilde{\epsilon}_b} \\ &\quad +\frac{\eta t}{2}\left(\frac{b}{\pi}\sum_{n=0}^{\infty}\frac{1}{2nb+\tilde{\epsilon}_b}\right)^2, \end{aligned} \quad \text{(A4)}$$

where n is the Landau-level index. Both terms are ultraviolet divergent, namely, at large n the sums diverge. An UV momentum cutoff was introduced for regularization as within the Langevin approach in Sec. II. To extract the divergent part, one can divide f_{gauss} into an infinite part with Λ and a finite part, u:

$$f_{\text{gauss}}=\frac{1}{2\pi}[\Lambda(\log\Lambda-1)+(\tilde{\epsilon}_b-b)\log\Lambda]+u(\tilde{\epsilon}_b,b). \quad \text{(A5)}$$

The finite part u can be simplified as

$$u(\tilde{\epsilon}_b,b)=\frac{b}{\pi}f_s(\tilde{\epsilon}_b/2b)+\frac{b}{\pi}(1/2-\tilde{\epsilon}_b/2b)\log(2b), \quad \text{(A6)}$$

where the function f_s is defined as

$$\begin{aligned} f_s(x) &= \log x-(x+1/2)[\log(x+1/2)-1]+\sum_{n=1}^{\infty}\left[\log(n+x)\right. \\ &\quad \left.-\int_{n-1/2}^{n+1/2}\log(y+x)dy\right], \end{aligned} \quad \text{(A7)}$$

which is basically $-\ln\Gamma(x)$ plus a constant. The total free energy within Gaussian variational approximation for all Landau levels is therefore,

$$\begin{aligned} f_{\text{gauss}}(\tilde{\epsilon}_b) &= \frac{1}{2\pi}\Lambda(\log\Lambda-1)-\frac{\eta t}{2}\left(\frac{1}{2\pi}\log\Lambda\right)^2+(\epsilon_b^r-b) \\ &\quad \times\left(\frac{1}{2\pi}\log\Lambda\right)+(\epsilon_b^r-b)u'+u+\frac{\eta t}{2}(u')^2. \end{aligned} \quad \text{(A8)}$$

Minimizing the energy, we get the gap equation

$$\epsilon_b^r=\tilde{\epsilon}_b-\eta t u'(\tilde{\epsilon}_b,b), \quad \text{(A9)}$$

consistent with the time-dependent approach [Eq. (36)].

Magnetization 2D can be obtained by taking the first derivative of Gibbs energy with respect to magnetic field b:

$$M_{2D}=-\frac{H_{c2}}{8\pi\kappa^2}\eta t\partial_b f_{\text{gauss}}=-\frac{e^*T}{2\pi\hbar cs}(\partial_b u-\eta t u'\partial_b u'). \quad \text{(A10)}$$

Similar calculation in 3D results in

$$M_{3D}=-\frac{e^*T}{2\pi\hbar c\xi_z}(\partial_b u_{3D}-\eta_{3D}tu'_{3D}\partial_b u'_{3D}). \quad \text{(A11)}$$

[1] A. Larkin and A. Varlamov, *Theory of Fluctuations in Superconductors* (Clarendon, Oxford, 2005).
[2] S. Ullah and A. T. Dorsey, Phys. Rev. Lett. **65**, 2066 (1990); S. Ullah and A. T. Dorsey, Phys. Rev. B **44**, 262 (1991).
[3] I. Ussishkin, S. L. Sondhi, and D. A. Huse, Phys. Rev. Lett. **89**, 287001 (2002).
[4] I. Ussishkin, Phys. Rev. B **68**, 024517 (2003).
[5] S. Mukerjee and D. A. Huse, Phys. Rev. B **70**, 014506 (2004).
[6] S. Tan and K. Levin, Phys. Rev. B **69**, 064510 (2004).
[7] T. T. M. Palstra, B. Batlogg, L. F. Schneemeyer, and J. V. Waszczak, Phys. Rev. Lett. **64**, 3090 (1990).
[8] J. A. Clayhold, A. W. Linnen, Jr., F. Chen, and C. W. Chu, Phys. Rev. B **50**, 4252 (1994).
[9] C. Hohn, M. Galffy, and A. Freimuth, Phys. Rev. B **50**, 15875 (1994).
[10] Z. A. Xu, N. P. Ong, Y. Wang, T. Kakeshita, and S. Uchida, Nature (London) **406**, 486 (2000).
[11] Y. Wang, Z. A. Xu, T. Kakeshita, S. Uchida, S. Ono, Y. Ando, and N. P. Ong, Phys. Rev. B **64**, 224519 (2001).
[12] Y. Wang, N. P. Ong, Z. A. Xu, T. Kakeshita, S. Uchida, D. A. Bonn, R. Liang, and W. N. Hardy, Phys. Rev. Lett. **88**, 257003 (2002).
[13] C. Capan, K. Behnia, Z. Z Li, H. Raffy, and C. Marin, Phys. Rev. B **67**, 100507(R) (2003).
[14] Y. Wang, L. Li, and N. P. Ong, Phys. Rev. B **73**, 024510 (2006).
[15] R. Bel, K. Behnia, and H. Berger, Phys. Rev. Lett. **91**, 066602 (2003); A. Pourret, H. Aubin, J. Lesueur, C. A. Marrache-Kikuchi, L. Berge, L. Dumoulin, and K. Behnia, Nat. Phys. **2**, 683 (2006); A. Pourret, H. Aubin, J. Lesueur, C. A. Marrache-Kikuchi, L. Berge, L. Dumoulin, and K. Behnia, Phys. Rev. B

76, 214504 (2007).
[16] H. Beidenkopf, N. Avraham, Y. Myasoedov, H. Shtrikman, E. Zeldov, B. Rosenstein, E. H. Brandt, and T. Tamegai, Phys. Rev. Lett. **95**, 257004 (2005); D. P. Li, B. Rosenstein, and V. Vinokur, J. Supercond. Novel Magn. **19**, 369 (2006).
[17] D. Li and B. Rosenstein, Phys. Rev. B **60**, 9704 (1999); **65**, 024513 (2001); **65**, 220504 (2002); **70**, 144521 (2004); Phys. Rev. Lett. **90**, 167004 (2003).
[18] D. J. Thouless, Phys. Rev. Lett. **34**, 946 (1975); G. J. Ruggeri and D. J. Thouless, J. Phys. F: Met. Phys. **6**, 2063 (1976); A. J. Bray, Phys. Rev. B **9**, 4752 (1974).
[19] N. Kokubo, K. Kadowaki, and K. Takita, Phys. Rev. Lett. **95**, 177005 (2005); N. Kokubo, T. Asada, K. Kadowaki, K. Takita, T. G. Sorop, and P. H. Kes, Phys. Rev. B **75**, 184512 (2007).
[20] W. E. Masker, S. Marcelja, and R. D. Parks, Phys. Rev. **188**, 745 (1969).
[21] N. R. Cooper, B. I. Halperin, and I. M. Ruzin, Phys. Rev. B **55**, 2344 (1997).
[22] H. Beidenkopf, T. Verdene, Y. Myasoedov, H. Shtrikman, E. Zeldov, B. Rosenstein, D. Li, and T. Tamegai, Phys. Rev. Lett. **98**, 167004 (2007).
[23] B. Rosenstein and V. Zhuravlev, Phys. Rev. B **76**, 014507 (2007).
[24] J. Y. Juang, M. C. Hsieh, C. W. Luo, T. M. Uen, K. H. Wu, and Y. S. Gou, Physica C **329**, 45 (2000).